Available online at www.sciencedirect.com
SCIENCE DIRECT®
Surface and Coatings Technology 182 (2004) 227–236
SURFACE & COATINGS TECHNOLOGY
www.elsevier.com/locate/surfcoat

Characterization of hydroxyapatite/nano-zirconia composite coatings deposited by high velocity oxy-fuel (HVOF) spray process

H. Li[a], K.A. Khor[a,*], R. Kumar[b], P. Cheang[b]

[a]*School of Mechanical and Production Engineering, Nanyang Technological University, 50, Nanyang Avenue, Singapore 639798, Singapore*
[b]*School of Materials Engineering, Nanyang Technological University, 50, Nanyang Avenue, Singapore 639798, Singapore*

Received 15 April 2003; accepted 11 August 2003

Abstract

Hydroxyapatite (HA)/nano-zirconia composite coatings were successfully produced through high velocity oxy-fuel (HVOF) spraying of radio frequency (RF) plasma synthesized powders. Microstructure characterization and morphology analysis on the nano-structured coatings were conducted using scanning electron microscopy (SEM), transmission electron microscopy (TEM), X-ray diffractometry (XRD), and differential scanning calorimetry (DSC). Elastic modulus of the coatings was determined using nano-indentation on polished cross-sections, which revealed Young's modulus value of ~130 GPa. Results also showed that the nano-sized zirconia particles (<90 nm) did not coarsen drastically after HVOF deposition, and were uniformly distributed throughout the coating. The crystallite size of tetragonal zirconia in the coating was found to be less than 13 nm. Furthermore, HA phase decomposition and chemical reaction between HA and zirconia was virtually undetected, which is beneficial towards the biological performance of the coatings. XRD analysis together with Rietveld refinement quantitatively revealed the content of the phases present in the coatings, including ~1.2 wt.% $CaZrO_3$. The conversion temperature of amorphous calcium phosphate to HA was found to be ~750 °C and the ancillary influence of the heat treatment on coating structure and properties were revealed.

Keywords: Hydroxyapatite; Zirconia; Nanostructured coatings; Ultrafine powders; Rietveld; Plasma synthesis; High velocity oxy-fuel (HVOF)

1. Introduction

The incorporation of bioinert ceramics, such as yttria stabilized zirconia (YSZ), alumina, and titania into a hydroxyapatite (HA) matrix has demonstrated significant improvement in mechanical properties [1–3] without substantial compromise in biocompatibility [4]. However, mutual reaction between calcium phosphates (CP) and YSZ seemed inevitable [2,3] and phase transformation of zirconia invariably took place during thermal spray coating deposition [5], which is detrimental on the basis that crystallographic transformation generated residual tensile stresses in the coating.

In recent years, nanostructured coatings attracted intense interest due to their enhanced mechanical properties [6,7]. The improvement can be related to the classical Hall–Petch relationship where decrease in particle size enhances the strength and toughness of ceramics [8,9]. Researchers have found that the main toughening mechanism in particulate reinforced composites was either crack inhibition or crack deflection [10]. Furthermore, a previous in vitro study has shown that nano-sized ceramics (Al_2O_3, TiO_2) possess significant capability of enhancing osteoblast adhesion on them [11]. Therefore, nano-sized particles within a biocompatible coating could bring about positive effects. However, available reports rely mostly on the rapid resolidification of sprayed materials upon their impingement on the prior deposited material, or substrate to form nano grains within the coating [7]. Even though nano-sized particles are produced through advanced powder synthesis techniques, the nano particles cannot be fed directly into a thermal spray gun to generate a nano-structured coating. Recent attempts involved forming agglomerates of nano particles into 30 μm aggregates [7,12]; however, excessive grain growth was

*Corresponding author. Tel.: +65-790-5526; fax: +65-791-1859.
E-mail address: mkakhor@ntu.edu.sg (K.A. Khor).

0257-8972/04/$ - see front matter © 2003 Elsevier Science B.V. All rights reserved.
doi:10.1016/j.surfcoat.2003.08.081

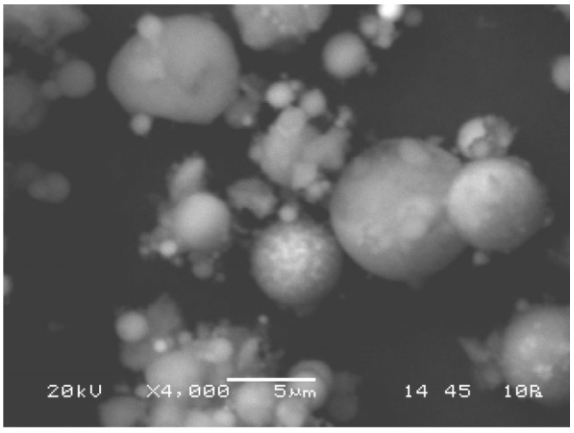

Fig. 1. Typical morphology of HA/nano-zirconia powders showing nano-sized zirconia particles attached to large HA particles.

discovered after coating deposition [12]. Meanwhile, recent attempts at sintering nano-size powders to form nano-structured bulk samples also encountered grain growth or density loss [13]. Therefore, a method to directly spray nano-sized particles to form nanostructured coating should be assiduously developed.

In the present study, HA/nano-zirconia powders synthesized in radio frequency (RF) plasma were sprayed using the high velocity oxy-fuel (HVOF) technique, which is of relatively low flame temperatures (<3000 °C) to assure limited heating of the powders. Nano-zirconia particulate reinforced coatings were obtained and their structure was characterized by scanning electron microscopy (SEM) and transmission electron microscopy (TEM). Furthermore, the effect of post-spray treatment on the coatings was investigated. Young's modulus of the coatings was determined using a nanoindentation test.

2. Materials and testing methods

The starting powders were prepared by suspension RF plasma spraying, as described in detail previously [14]. A nano-sized zirconia (ZrO_2) suspension was initially mixed with a solution, which was utilized for HA preparation by a wet chemical method [14]. This mixture was subsequently fed axially into the RF plasma to form novel HA/nano-zirconia composite powders of composition 90 wt.% HA + 10 wt.% zirconia. In order to get the powders in a particle size range suitable for HVOF spray, the agglomerated powders were sieved to a size range of $-120+20$ μm. The size distribution of the sieved RF powders, determined by a laser particle size analyzer (Analysette 22, Fritsch GmbH, Germany), showed that the average diameter of the powder aggregates was ~40 μm. A fully computerized HV2000 HVOF system (Praxair, USA) with a nozzle diameter of 19 mm was employed for the coating deposition on grit-blasted Ti-6Al-4V substrates. Hydrogen was the fuel gas while the powder carrier gas was argon. The flow rates of oxygen, hydrogen and argon were 283 l/min, 566 l/min and 19 l/min, respectively. The spray distance was 250 mm and powder feed rate was 6 g/min. SEM observation on the powders before sieving (Fig. 1) shows that the powders are promising in the sense that nano-zirconia particles attached onto large calcium phosphate (CP) particles without obvious changes in size. Phase analysis by X-ray diffraction (XRD) revealed the presence of crystalline HA, amorphous calcium phosphate (ACP), α-tricalcium phosphate (α-TCP), tetragonal zirconia (t-ZrO_2), and $CaZrO_3$ (Fig. 2). XRD plots of other coatings, in this study, are also demonstrated in Fig. 2 for comparison, which will be discussed later. Relative phase composition of all the phases was determined via the Rietveld method [15]. Alumina powder (<5 μm in diameter) with fixed weight percentage was added to the starting HA/nano-zirconia powders and crushed coating samples (containing ACP) for calibration purpose since Rietveld technique is only valid for samples with high crystallinity ($>95\%$). 1.0 wt.% of $CaZrO_3$ within the starting powders was determined. Moreover, the crystallinity was appraised using the XRD pattern analysis [16] and a crystallinity level of 83% was found in the starting powders. Ti-6Al-4V plates ($60\times40\times2$ mm^3) were utilized as substrates for coating deposition.

Coating microstructure was analyzed on polished cross-sections using SEM (JEOL, JSM-5600LV) and TEM (JEOL, JEM-2010 operating at 200 kV). Differential scanning calorimetry (DSC) (Netzsch Thermal Analysis, DSC 404C) was utilized for the thermal behavior investigation of the powders and coatings at elevated temperatures. DSC test used nitrogen gas as the atmosphere with the flow rate of 150 ml/min; the

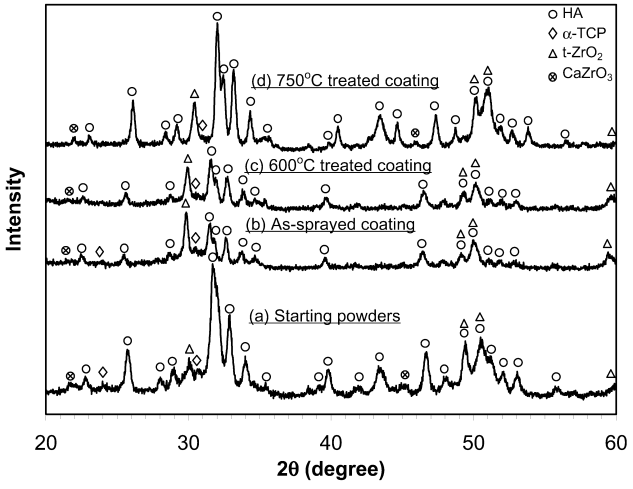

Fig. 2. XRD patterns of the starting powders, as-sprayed coating, 600 °C treated coating, and 750 °C treated coating.

heating rate was 5 °C/min. The phase composition of the starting powders and as-sprayed coatings was analyzed by means of XRD (MPD 1880, Philips, The Netherlands). The operating conditions were 40 kV and 30 mA by using Cu Kα radiation. The goniometer was set at a scan rate of 0.02°/s over the 2θ range 20–80°. Young's modulus of the investigated coatings was determined on polished cross-sections of the coatings using the Nano-Indenter®XP system. For each test, a total of 15 points were collected and averaged. The load used for nanoindentation was 100 mN. The heat treatment on the as-sprayed coatings was conducted within an electrical resistant furnace with a heating rate of 15 °C/min and duration of 30 min at peak temperature. Furthermore, in vitro testing of the coatings was conducted to reveal their bioactivity.

3. Results and discussion

The XRD pattern of the as-sprayed HA/nano-zirconia coating (Fig. 2) suggests the appearance of $CaZrO_3$, apart from crystalline HA, α-TCP, and t-ZrO_2. It is noted that, owing to the rapid cooling of the powders during processing, m-ZrO_2 was not present within both the starting powders and coatings. Extensive studies have been conducted to clarify the phase transformation mechanisms of HA during thermal spraying. It was well accepted that α-TCP resulted from the transformation shown as follows above 1000 °C [17], or upon a small temperature range thereof, depending on the heating environment [18,19], which was stated to be the starting temperature of HA decomposition,

$$Ca_{10}(PO_4)_6(OH)_2 \rightarrow 3Ca_3(PO_4)_2 + CaO + H_2O \quad (1)$$

In a previous study [16], the decomposition was found to take place mainly within the partially molten portion of HA deposits. In the present study, partially molten state of the CP particles was also revealed through SEM observation on the as-sprayed particles and a crystallinity of 74% of the as-sprayed coating is revealed. Compared to previous reports [20,21], transformation of HA is limited since no β-TCP, TTCP, or other phases were detected, that are part of the complex phase transformation within thermal sprayed calcium phosphates. The results indicate the temperatures of HA particles attained in the HVOF flame. Nevertheless, the content of TCP can be effectively utilized to evaluate the extent of HA decomposition during coating deposition. The presence of $CaZrO_3$ suggests a reaction between HA and zirconia during powder preparation and coating deposition. The quantitative contents of all the contributing phases in the samples demonstrated in Table 1 reveal a decrease of zirconia by 1.2 wt.% and an increase of $CaZrO_3$ by 0.2 wt.%. The decrease of t-ZrO_2 content, from originally 10 wt.% before RF plasma spraying to 9.3 wt.%

Table 1
Content of the phases present in the starting powders and coatings determined using the Rietveld refinement

	α-TCP	t-ZrO_2	$CaZrO_3$	HA + ACP
Powders	6.7	9.3	1.0	Bal.
As-sprayed coating	7.5	8.1	1.2	Bal.
600 °C treated coating	7.5	8.1	1.2	Bal.
750 °C treated coating	7.5	8.1	1.2	Bal.

in the spray powders resulted mainly from the chemical reaction to form $CaZrO_3$ during powder preparation and partially from the sieving process. According to the well-recognized phase transformations exhibited by the main polymorphic forms of zirconia, monoclinic $\overset{1150\ °C}{\underset{950\ °C}{\rightleftarrows}}$ tetragonal $\overset{2370\ °C}{\leftrightarrow}$ cubic $\overset{2680\ °C}{\leftrightarrow}$ liquid, it is obvious that the absence of m-ZrO_2 could be attributed to the insufficient heating of zirconia particles during the HVOF spraying. Additionally, the extremely small particle size of the zirconia was reported to be responsible for the lack of transformation from t→m-ZrO_2 [22,23] together with other factors, such as rapid cooling the particles upon impingement and residual stress formed at HA/zirconia zone during quenching of melted CP. Phase transformation of zirconia during thermal spraying, especially during plasma spraying [5,24,25], is detrimental to the coating properties, because of generation of residual stresses and microcracks. The absence of transformation of t-ZrO_2 is beneficial to the coating since t-ZrO_2 has high strength, high toughness and excellent resistance against impact. Especially for the implant coating, high toughness is important since the implant prosthesis must be reliable in the presence of body fluids and complex local loading. Therefore, the present HVOF technique is a preferable method for such coating deposition.

The equilibrium ZrO_2–CaO phase diagram [26] depicted in Fig. 3 illustrates possible reactions between ZrO_2 and CaO in detail. It shows that, under the equilibrium conditions, heating of the zirconia particles up to 1140 ± 40 °C caused transformation to a mixture of t-ZrO_2 and c-ZrO_2. The present results claim the absence of m-ZrO_2, which indicates that the t-ZrO_2 and possibly c-ZrO_2 particles in the coating are sufficiently stabilized through solid solution of CaO in ZrO_2 and these phases are effectively retained following rapid quenching during the coating deposition. Moreover, the present study also reveals the absence of $CaZr_4O_9$ and $Ca_6Zr_{19}O_{44}$ owing mainly to the small content of CaO. Even though the phase diagram (Fig. 3) cannot be convincingly used to explain the phenomena that actually occurred during the coating formation, it can be

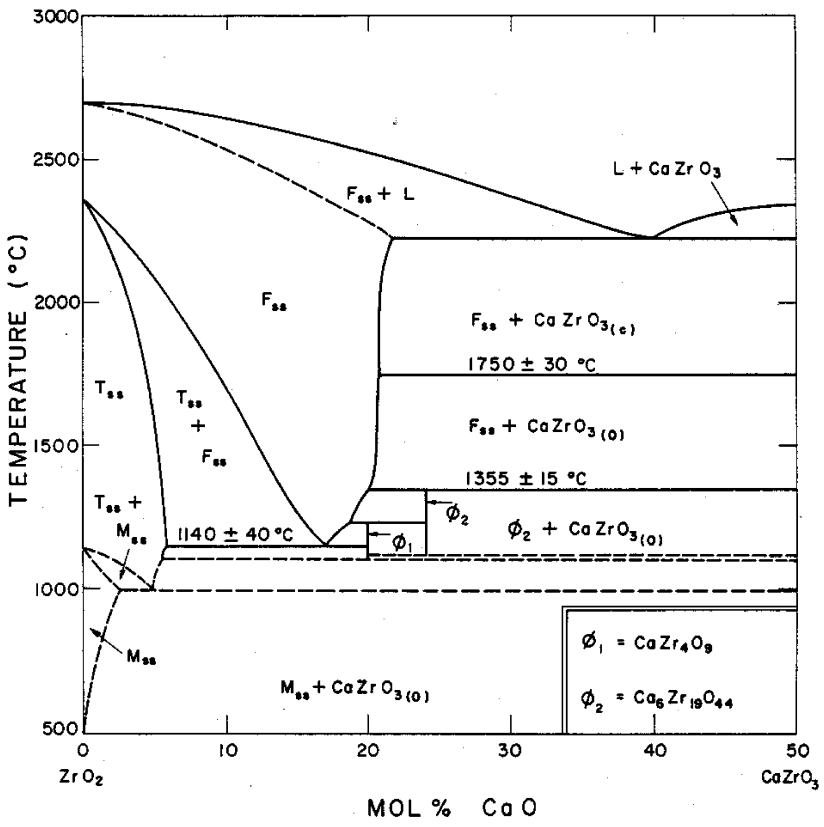

Fig. 3. ZrO_2–CaO phase diagram [26], T_{ss}–tetragonal solid solution, M_{ss}–monoclinic solid solution, F_{ss}–cubic solid solution, *L*–liquid.

used, more or less, to understand the behavior between zirconia and CaO. Furthermore, as it has been found that HA decomposition to other phases, e.g. CaO, takes place beyond 1000 °C, the gradually increased content of CaO in the present zirconia/HA system makes the reactions between zirconia and CaO more complicated. The small content change exhibited by α-TCP (increased from 6.7 to 7.5 wt.%) has indicated the low content of CaO according to Eq. (1). It was pointed out that CaO reacts preferentially with t-ZrO_2 to form $CaZrO_3$ [27], which can be described as follows,

$$CaO + \text{t-}ZrO_2 \rightarrow CaZrO_3. \quad (2)$$

The present spray powders exhibit the main component of t-ZrO_2, which is beneficial for the reaction. As observed from Fig. 1, within the starting powders, CP particle and nano-zirconia particles must bond together through a reaction layer (chemical bond) formed during powder preparation. Such reaction between HA and zirconia particles can be demonstrated using the same model proposed in a previous paper reporting on HA/titania composite coating [28]. Quantitative phase analysis on the samples, which was shown in Table 1, reveals the increase of $CaZrO_3$ content in the as-sprayed coating compared to that in the powders. It hence indicates that further reaction between HA and zirconia took place during coating formation (approx. 13% intensified according to the loss of t-ZrO_2). However, it is well known that HVOF flame temperature is relatively low, <3000 °C, hence the extent of the reaction is rather limited, which further reveals the suitability of HVOF technique for such coating deposition.

SEM observation on the coating shows evidence that a dense composite structure was produced with evenly distributed zirconia particles (Fig. 4). The incorporation of zirconia (the bright long tapes shown in Fig. 4b, they are located at the HA splats' interface) results in obvious increase in density, in other words, decreased porosity (obtained from morphology analysis) compared to HVOF sprayed pure HA coatings (Fig. 4a). Further morphology investigation, which is typically shown in Fig. 5, reveals formation mechanism of micropores within the coating. The micropores with the size of less than 2 μm formed during splat formation within the melted zone of a HA particle. Since it is generally believed that the impingement-resolidification behavior of a single splat is an isolated procedure, such pores contribute principally to the final porosity of the bulk coating. The pores within the splat may result from evaporation or release of entrapped gases within the droplets during the HVOF spray, which come mainly from pre-existed micropores in the porous HA particles

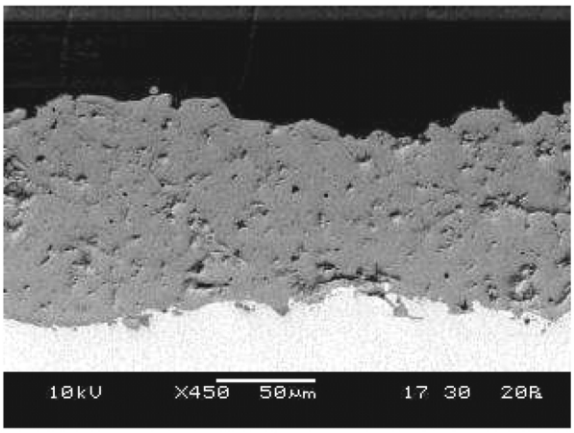

Fig. 4. Typical cross-sectional microstructure of the HVOF sprayed (a) pure HA coating and (b) HA/nano-zirconia coating showing an improved structure brought about by the incorporation of zirconia.

and entrained air between the splat and substrate or pre-coating before complete resolidification. These pores can be effectively sealed through in-filling by subsequent droplets that impinged on prior deposited material. Therefore, the nano-sized zirconia particles located around HA particles' surface (Fig. 1) could be beneficial for the pore-sealing effect. This could be the main reason why the composite coating shows an improved mechanical property.

Further observation with TEM reveals the nano-sized zirconia particles in the coating (Fig. 6a). High magnification observation of a cluster of zirconia particles (Fig. 6b) shows t-ZrO_2 grains with an average diameter of less than 13 nm. The selected area diffraction (SAD) pattern (Fig. 6c) confirms the nano-sized zirconia particles with a tetragonal structure. It is suggested that the nano-sized zirconia particles did not coarsen appreciably during HVOF spray, which indicates limited heating by the HVOF flame of these particles. Distinct crystallographic orientation relations between the reaction product $CaZrO_3$ and zirconia have been reported within the composites of HA and large zirconia powder particles (0.2 μm): $[012]ZrO_2//[\bar{3}23]CaZrO_3$], and $(200)ZrO_2//(101)$ $CaZrO_3$ [29]. However, in the present study, such relation was not detected since the reaction between HA and zirconia is very limited. Nevertheless, the reaction between t-ZrO_2 and CaO is effectively influenced by the extent of the decomposition of HA represented in Eq. (1), which provides the reaction components. The novel HA/nano-zirconia powders showed a capability of effectively inhibiting mutual reaction among the resident phases, and hence are suitable for coating deposition.

To clarify the thermal behavior of the powders and coatings at elevated temperatures, a high temperature DSC test was conducted. Fig. 7 demonstrates the DSC heating curves of the samples compared to pure crystalline HA powder. The HA powder, HA/nano-ZrO_2 powder and the crushed nano-composite coating exhibit various diverse chemical changes except the peak labeled at approximately 1450 °C. The peak labeled at 1442–1450 °C on the curves is assigned to further transformation of CP phases [30,31]. It is noted that HA powders exhibit the endothermic characteristic during heating, which spans approximately from 1180 to 1340 °C. These broad peaks may refer to the decomposition of HA to α-TCP or even $Ca_4O(PO_4)_2$ [30,32]. Beyond 1200 °C, HA loses its OH^- groups gradually [30]. The exothermic peak at 865.5 °C on the curve referring to the as-sprayed coating may be related to the recrystallization of ACP. Under equilibrium conditions (Fig. 3), the reaction between HA and t-ZrO_2 can take place at low temperatures ($\ll$1000 °C). In the present system, the reaction, however, should occur only as the powder temperature is higher than 1000 °C since CaO can only

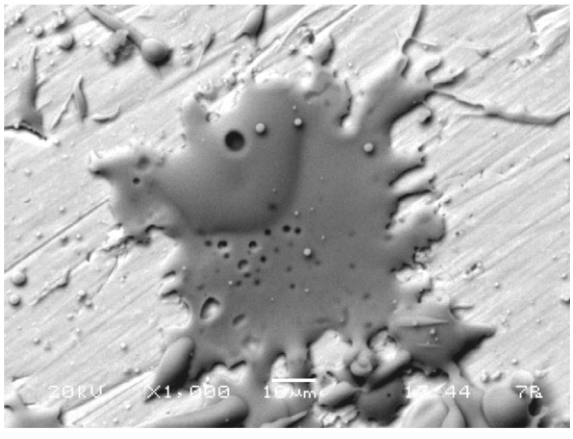

Fig. 5. SEM image of a single HA splat indicating the formation mechanism of micropores within a coating. The splat was prepared through HVOF spraying pure HA particle onto polished Ti6Al4V substrate using the same spray parameters as for the present composite coating.

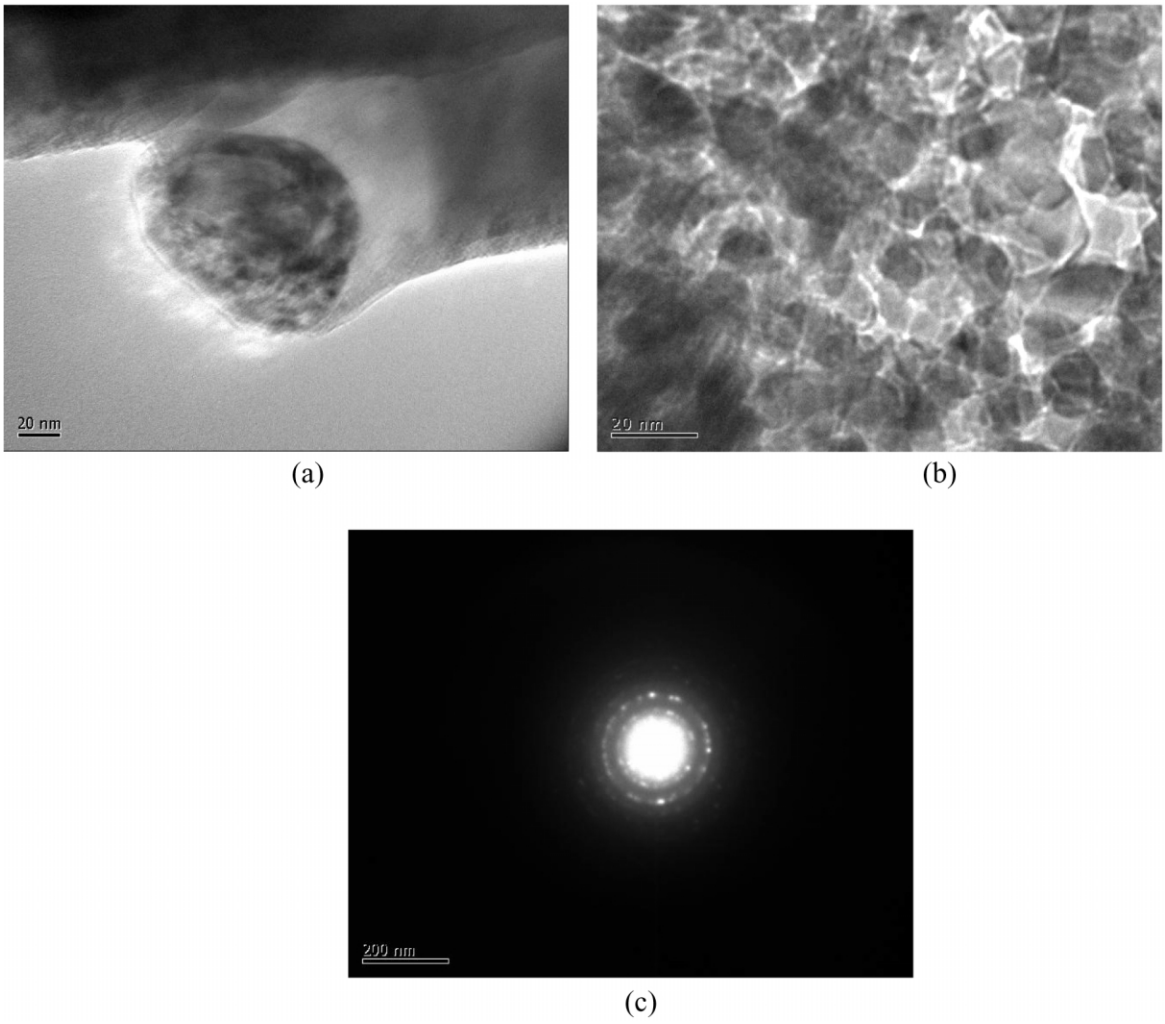

Fig. 6. TEM images of the HA/nano-zirconia coating, (a) shows a nano t-ZrO_2 particle (approx. 85 nm in diameter), (b) shows a cluster of nano-sized t-ZrO_2 grains (<13 nm), and (c) SAD pattern confirms the nano-sized zirconia grains with tetragonal structure from [010] zone.

be released from HA transformation beyond that point. Unfortunately, the present DSC system used is not sensitive enough to reveal pertinent information on this reaction.

Concerning the influence of heating rate [33] and heating circumstance (e.g. humidity, etc. [34]) on the recrystallization temperature of the ACP together with previous investigation on pure HA coating [35], the coatings were heat treated at 750 and 600 °C for comparison. The samples were heated in an annealing furnace with a heating rate of 15 °C/min, held for 30 min, and then slowly cooled to room temperature in the furnace. The heating and cooling was performed in air. The effect of post-spray heat treatment on the phase composition of the coatings was already shown in Fig. 2c,d. It is noted that post-spray annealing at 600 °C did not cause any changes in the phase composition, especially in terms of crystallinity, while the 750 °C treatment achieves full crystallization. Moreover, compared

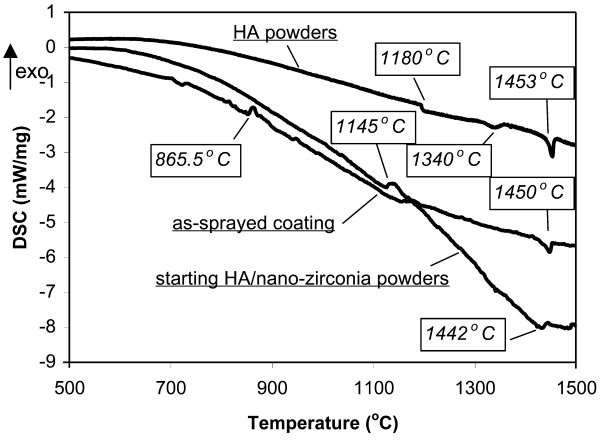

Fig. 7. DSC heating curves of the powders and as-sprayed coatings with comparison to pure crystalline HA powders.

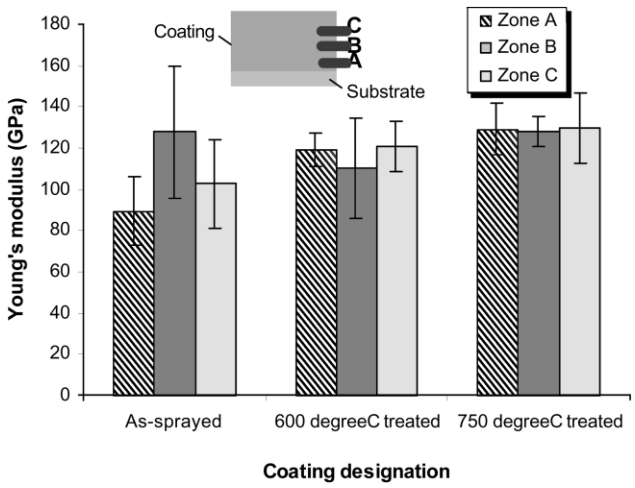

Fig. 8. Young's moduli of the HA/nano-zirconia coatings determined by nano-indentation test on the coating cross-sections showing the influence of heat treatment and different locations.

to the as-sprayed coating, the heat treatment induced no supplementary reaction between HA and zirconia, indicated by the essentially unchanged t-ZrO_2 content. Likewise, the unchanged content of α-TCP induced by the recrystallization treatment within the coatings corresponds to previous findings that the transformation of ACP to HA did not significantly influence the α-TCP content [35].

The effect of the post-spray treatment on Young's modulus (E) of the coatings is shown in Fig. 8. As depicted in the figure, zones A, B, and C correspond to the locations near the coating/substrate interface, approximate mid-layer of the coating, and the top layer of the coating. The coatings can reach an E value of 130 GPa, and the results indicate the significant influence of coating structure on coating property. Different areas within the as-sprayed coating exhibit significantly different E values ($P<0.05$ according to paired Student's t-distribution analysis [36]). It has been pointed out, and is reasonable that the coatings near to coating/substrate interface should contain more ACP and other phases transformed from HA owing to faster cooling rate than those far from the interface [37]. The diminished difference in E values exhibited by heat treated coating (600 °C, 30 min) together with unchanged phase composition illustrated in Table 1 suggests possible influence of residual stresses within the coating, which were found generally to be tensile in nature [38,39]. The low Young's modulus exhibited by the upper layer of the as-sprayed coating compared to that of the middle layer also indicates the possible influence of residual stresses on local Young's modulus. It is believed that the residual stress could play an identified role in influencing E value through, as reported [38,40], influencing microcracking within the coating. Combining with the available coating residual stress analysis [39], which shows a decreased trend of the tensile stresses from the layer far from interface to that close to the interface, the present study suggests that tensile stress could be detrimental towards attaining a high Young's modulus value. Together with the comparative results revealed from the heat-treated coating, the increased E values confirm that the ACP should be of lower E value than crystalline HA. The unique E values within the crystallized coatings imply the extermination of both the residual stress, which is obviously achieved through the prolonged high temperature annealing, and difference in phase composition. Furthermore, recrystallization treatment eliminates the influence of hardening effect on the coating induced by rapid cooling during coating formation. However, the unique result also claims the aforementioned assumption, that is, the difference in phases, and residual stresses both influence the E values. Furthermore, remarkable HA grain growth induced by recrystallization heat-treatment was also revealed through the TEM observation (increased from approx. ~80 μm to ~170 μm). The changes in grain size could also contribute to the altered mechanical performances of the bulk coatings.

According to Sih [41], once a crack is initiated the fracture path within a material sample follows the trajectory of points of minimum strain energy density remarkably well. TEM observation on the composite coating (Fig. 9) shows that the crack penetrates through HA grains rather than propagating along grain interfaces. It is known that calcium phosphates are brittle, and addition of zirconia improves the ductility at HA/zirconia interface, which could be beneficial towards an improved crack-inhibiting capability. Among the struc-

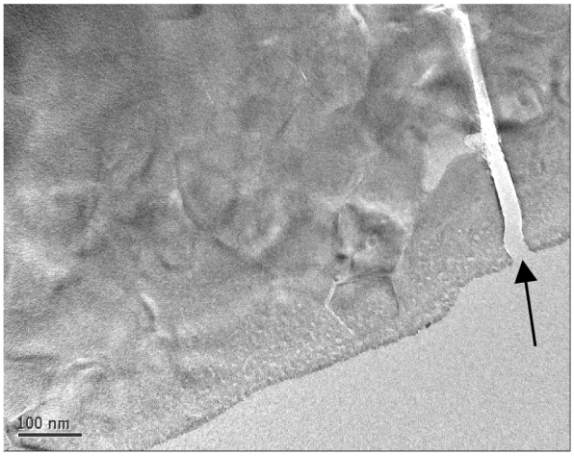

Fig. 9. TEM image of the HA/nano-zirconia coating showing a crack penetrating through a HA grain rather than along grain boundaries. The crack was formed during thin-foil preparation. The arrow refers to the grain-penetrating crack.

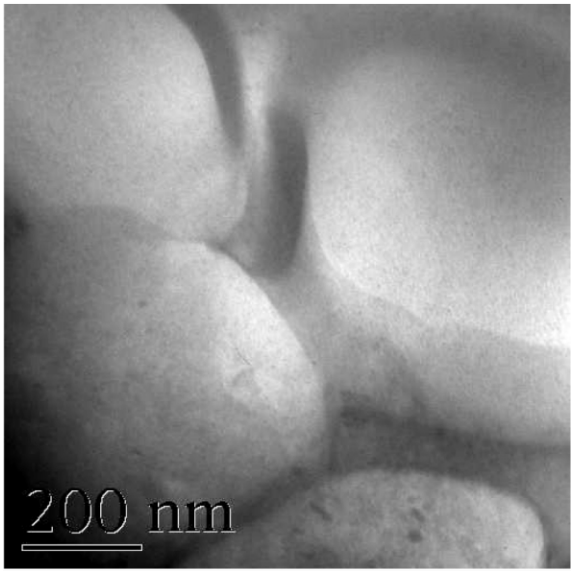

Fig. 10. TEM image of HVOF sprayed pure HA coating showing the poor bonding state between calcium phosphate splats. The amorphous grain-boundary phase is visible between the grains.

ture variables, the size and distribution of pores were reported to play a major role in influencing the initiation and propagation processes of cracks [42], and hence significantly influence coating properties [43]. Furthermore, it has been reported that propagation of the cracks through the particulate reinforcements or grains or grain boundaries predominantly depended on crack propagation velocity and relative extent of thermal mismatch, and elastic modulus mismatch among the components [44]. From the morphology observation, it was revealed that the incorporation of the nano-sized zirconia improved the structure of the HA-based coatings, the presence of zirconia particles at unbonded area between HA splats can improve the structure (Fig. 4b). The improved structure is useful for the enhancement of fracture property according to following formula, which correlates the porosity and effective fracture toughness [45]:

$$k_{\mathrm{Ic}}^{\mathrm{eff}} = k_{\mathrm{Ic}}\sqrt{m} \tag{3}$$

where $m = 1 - \lambda/\varepsilon$, λ/ε is the porosity along the crack propagation path, λ and ε are dimensionless parameters representing dimensionless diameter of simulated circular microvoids and dimensionless distance between the center of two voids, respectively. It is believed that the crack growth was accelerated by successive sudden jumps at each void along the crack path. Other researchers also reported the negative effect of micropores on the fracture toughness of HA/YSZ composites [46]. For HVOF-sprayed pure HA coatings made from 40 μm HA powders using the same spray parameters, the area

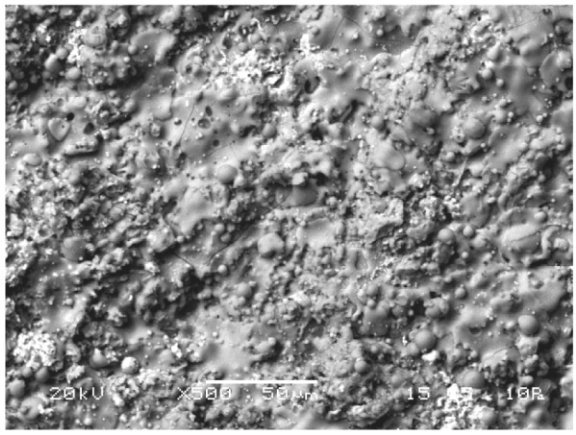

(a)

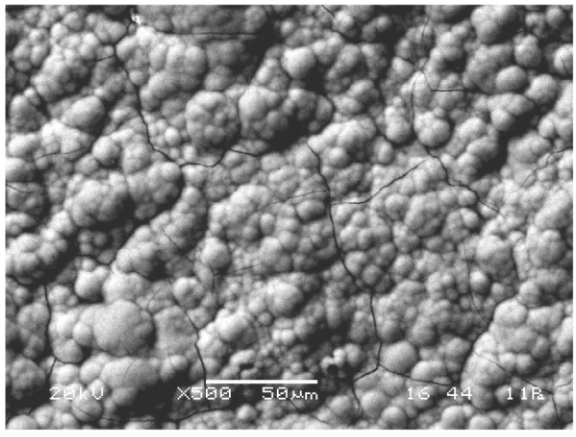

(b)

Fig. 11. Typical surface morphology of the as-sprayed HA/nano-zirconia coating (a) and the coating aged in the SBF with 3 days (b) showing the precipitation of the bone-like apatite.

at the CP splats' interface indicates a poor bonding state (Fig. 10). Also, the amorphous phase (ACP) between the HA grains is evident from the observation of the TEM image. It is not surprising that with the increase of nano-zirconia content, the mechanical properties of the HA/nano-zirconia coatings would be further improved on a basis that the nano-sized zirconia would strengthen the CP grain boundaries.

Since the final purpose of the HA/nano-zirconia coatings is to be used for hard tissue replacement, in vitro test is a necessary process to evaluate the changes of the material in simulated body fluid (SBF). The details of the in vitro testing, including sample dimension, procedures, etc., have already been described in a previous report [47]. The coating samples were incubated in a SBF solution in accordance to Kokubo's protocol. It was found that after 3 days of incubation, a bone-like apatite layer precipitated on the HA/nano-

zirconia coating surface (Fig. 11), which suggests satisfactory bioactivity of the coatings.

4. Conclusions

Novel nanostructured HA/nano-zirconia coatings were successfully deposited by HVOF spray using RF plasma synthesized powders as feedstock. Subsequent characterization of the coatings revealed no obvious phase changes from the primary powder's phase composition. The uniformly dispersed nano-sized zirconia particles in the HA-based coatings did not coarsen drastically following the HVOF spray deposition. Limited reaction between HA and zirconia was found in the coating, which is mainly due to thermal decomposition of HA in the HVOF flame. Heat treatment of the HA/nano-zirconia coating at 750 °C and 30 min improved the homogeneity of the coatings through equalizing the phase compositions and achieved uniform Young's modulus throughout the nanostructured coating. The Young's modulus of the coating was found to attained a maximum value of ~130 GPa. The present study suggests that RF plasma processing is a valuable tool for nanostructured powder preparation, and, commensurate with HVOF spray of nano-structured coating.

Acknowledgments

Financial support by Agency for Science, Technology and Research (A*STAR), Singapore in the form of a research grant Project No.: 034 101 012 is acknowledged.

References

[1] W.J. Chang, B.C. Wang, C.Y. Yang, J. Mater. Sci. Mater. Med. 8 (1997) 193.
[2] L. Fu, K.A. Khor, J.P. Lim, J. Am. Ceram. Soc. 85 (2002) 800.
[3] H. Kurzweg, R.B. Heimann, T. Troczynski, W.L. Wayman, Biomaterials 19 (1998) 1507.
[4] E. Chang, W.J. Chang, B.C. Wang, C.Y. Yang, J. Mater. Sci. Mater. Med. 8 (1997) 201.
[5] C.H. Lee, H.K. Kim, H.S. Choi, H.S. Ahn, Surf. Coat. Technol. 124 (2000) 1.
[6] Y.C. Zhu, K. Yukimura, C.X. Ding, P.Y. Zhang, Thin Solid Films 388 (2001) 277.
[7] C.C. Berndt, (Ed.), Thermal spray processing of nanoscale materials II – extended abstracts, J. Therm. Spray Technol. 10 (2001) p. 147.
[8] M. Wang, R. Joseph, W. Bonfield, Biomaterials 19 (1998) 2357.
[9] S.K. Kim, H.J. Yoo, Surf. Coat. Technol. 109 (1998) 564.
[10] S. Ranganath, J. Mater. Sci. 32 (1997) 1.
[11] T.J. Webster, R.W. Siegel, R. Bizios, Biomaterials 20 (1999) 1221.
[12] R.S. Lima, A. Kucuk, C.C. Berndt, Mater. Sci. Eng. A313 (2001) 75.
[13] M.R. Towler, I.R. Gibson, S.M. Best, J. Mater. Sci. Lett. 19 (2000) 2209.
[14] R. Kumar, P. Cheang, K.A. Khor, J. Mater. Process. Technol. 113 (2001) 456.
[15] R.A. Young, The Rietveld Method, Int. Union of Crystallography, Oxford University Press, New York, 1993.
[16] H. Li, K.A. Khor, P. Cheang, Mater. Sci. Eng. A293 (2000) 71.
[17] C. Liao, F. Lin, K. Chen, J. Sun, Biomaterials 20 (1999) 1807.
[18] P.E. Wang, T.K. Chaki, J. Mater. Sci. Mater. Med. 4 (1993) 150.
[19] J. Zhou, X. Zhang, J. Chen, S. Zeng, K. de Groot, J. Mater. Sci. Mater. Med. 4 (1993) 83.
[20] R. McPherson, N. Gane, T.J. Bastow, J. Mater. Sci. Mater. Med. 6 (1995) 327.
[21] D.M. Liu, H.M. Chou, J.D. Wu, J. Mater. Sci. Mater. Med. 5 (1994) 147.
[22] M. Ruhle, A.H. Heuer, Phase transformations in ZrO_2-containing ceramics: II, the martensitic reaction, advances in ceramics, in: N. Claussen, M. Ruhle, A. Heuer (Eds.), Science and Technology of Zirconia, 12, The American Ceramic Society, Inc, Ohio, USA, 1984, pp. 14–32.
[23] C.A. Andersson, T.K. Gupta, Phase stability and transformation toughening in zirconia, advances in ceramics, in: A.H. Heuer, L.W. Hobbs (Eds.), Science and Technology of Zirconia, 3, The American Ceramic Society, Inc, Ohio, USA, 2001, pp. 184–201.
[24] T. Chraska, A.H. King, Thin Solid Films 397 (2001) 30.
[25] R.W. Trice, Y.J. Su, K.T. Faber, H. Wang, W. Porter, Mater. Sci. Eng. A272 (1999) 284.
[26] V.S. Stubican, Phase equilibria and metastabilities in the systems ZrO_2–MgO, ZrO_2–CaO, and ZrO_2–Y_2O_3, advances in ceramics, in: S. Somiya, N. Yamamoto, H. Hanagida (Eds.), Science and Technology of Zirconia III, 24A, The American Ceramic Society, Inc, Ohio, USA, 1998, pp. 71–82.
[27] R.R. Rao, T.S. Kannan, Mater. Sci. Eng. C20 (2002) 187.
[28] H. Li, K.A. Khor, P. Cheang, Biomaterials 24 (2003) 949.
[29] B.Y. Chou, E. Chang, S.Y. Yao, J.M. Chen, J. Am. Ceram. Soc. 85 (2002) 661.
[30] H. Aoki, Medical Applications of Hydroxyapatite, Ishiyaku EuroAmerica, Inc, Tokyo, St. Louis, 1994.
[31] J. Zhou, X. Zhang, J. Chen, S. Zeng, K. de Groot, J. Mater. Sci. Mater. Med. 4 (1993) 83.
[32] M. Ogiso, Y. Yamashita, T. Matsumoto, J. Biomed. Mater. Res. 41 (1998) 296.
[33] C.F. Feng, K.A. Khor, S.W.K. Kweh, P. Cheang, Mater. Lett. 46 (2000) 229.
[34] K.A. Gross, V. Gross, C.C. Berndt, J. Am. Ceram. Soc. 81 (1998) 106.
[35] H. Li, K.A. Khor, P. Cheang, Biomaterials 23 (2002) 2015.
[36] A.J. Hayter, Probability and Statistics, PWS Publishing Company, USA, 1996.
[37] K.A. Gross, C.C. Berndt, J. Biomed. Mater. Res. 39 (1998) 580.
[38] Y.C. Tsui, C. Doyle, T.W. Clyne, Biomaterials 19 (1998) 2015.
[39] Y. Han, J. Nan, K. Xu, J. Lu, J. Mater. Sci. Lett. 18 (1999) 1087.
[40] V. Sergo, O. Sbaizero, D.R. Clarke, Biomaterials 18 (1997) 477.
[41] G.C. Sih, Mechanics of Fracture Initiation and Propagation, Kluwer Academic Publishers, USA, 1991.

[42] S. Ishihara, A.J. Mcevily, T. Goshima, K. Kanekasu, T. Nara, J. Mater. Sci. Mater. Med. 11 (2000) 661.
[43] I. Sevostianov, M. Kachanov, Mater. Sci. Eng. A297 (2001) 235.
[44] P. Bhargava, B.R. Patterson, J. Am. Ceram. Soc. 80 (1997) 1863.
[45] D. Leguillon, Influence of micro-voids on toughness of interfaces, in: (Ed.), Damage and Failure of Interface, Balkema, Rotterdam, 1997, pp. 113–120.
[46] Y. Yamada, R. Watanabe, Scr. Mater. 34 (1996) 387.
[47] K.A. Khor, H. Li, P. Cheang, S.Y. Boey, Biomaterials 24 (2003) 723.